European Journal of Remote Sensing

ISSN: (Print) 2279-7254 (Online) Journal homepage: http://www.tandfonline.com/loi/tejr20

Automatic refocus and feature extraction of single-look complex SAR signatures of vessels

Luis E. Yam & Jordi J. Mallorqui

To cite this article: Luis E. Yam & Jordi J. Mallorqui (2016) Automatic refocus and feature extraction of single-look complex SAR signatures of vessels, European Journal of Remote Sensing, 49:1, 745-758

To link to this article: http://dx.doi.org/10.5721/EuJRS20164939

European Journal of Remote Sensing - 2016, 49: 745-758
doi: 10.5721/EuJRS20164939
Received 12/02/2016 accepted 28/07/2016

European Journal of Remote Sensing
An official journal of the Italian Society of Remote Sensing
www.aitjournal.com

Automatic refocus and feature extraction of single-look complex SAR signatures of vessels

Luis E. Yam* and Jordi J. Mallorqui

Department of Signal Theory and Communications (TSC), Universitat Politècnica de Catalunya (UPC), C/ Jordi Girona 1-3, 08034, Barcelona, Spain
*Corresponding author, e-mail address: eduardo.yam@tsc.upc.edu

Abstract
In recent years, spaceborne synthetic aperture radar (SAR) technology has been considered as a complement to cooperative vessel surveillance systems thanks to its imaging capabilities. In this paper, a processing chain is presented to explore the potential of using basic stripmap single-look complex (SLC) SAR images of vessels for the automatic extraction of their dimensions and heading. Local autofocus is applied to the vessels' SAR signatures to compensate blurring artefacts in the azimuth direction, improving both their image quality and their estimated dimensions. For the heading, the orientation ambiguities of the vessels' SAR signatures are solved using the direction of their ground-range velocity from the analysis of their Doppler spectra. Preliminary results are provided using five images of vessels from SLC RADARSAT-2 stripmap images. These results have shown good agreement with their respective ground-truth data from Automatic Identification System (AIS) records at the time of the acquisitions.
Keywords: SAR, autofocus, vessel detection, feature analysis, surveillance.

Introduction
Synthetic Aperture radar (SAR) is a widespread technique used in the microwave remote sensing community for acquiring images of the Earth's surface over any location. Current civilian spaceborne SAR sensors such as RADARSAT-2, TerraSAR-X or Sentinel-1 are able to provide high-resolution images that allow the identification of man-made objects. These sensors give rise to a wide range of possibilities for the development and analysis of algorithms for extracting special features from the SAR data, allowing the detection and classification of a variety of targets of interest.
In recent years, spaceborne SAR sensors have been considered an interesting source of information for vessel surveillance systems due to their imaging capabilities [Crisp, 2004; Estable et al., 2009; Brusch et al., 2011; Margarit, 2013]. These types of sensors are able to obtain images over any area of interest of the sea surface regardless of the weather conditions and natural illumination. In addition, they act as non-cooperative detection systems, i.e. the detection is performed without acknowledgment of the targets. Thanks to

these characteristics, the spaceborne SAR sensors can complement traditional cooperative monitoring systems such as the Automatic Identification System (AIS) [IMO, 2015] or the Vessel Monitoring System (VMS) [European Commission, 2015]. In addition, the use of SAR images would also expand their coverage farther from the coast line and provide information for data correlation in order to highlight suspicious activities.

While the vessel detection techniques using SAR images have achieved a level of refinement which presents low false alarm rates [Crisp, 2004; Tello et al., 2005; Staglianò et al., 2014], the classification and feature extraction algorithms still face great challenges related with the complex behaviour of the SAR signatures of the vessels. The extraction of the vessels' features has been an active area of research to obtain useful information for monitoring systems like dimensions, heading, and speed. In the case of single-channel SAR images, the extraction of the dimensions of a vessel are typically obtained by, first, isolating its SAR signature using a constant false rate alarm (CFAR) approach, and then, computing its respective bounding box [Brusch et al., 2011; Estable et al., 2011; Zang et al., 2013]. Thus, a key factor of this procedure is the proper model of the sea clutter for the correct discrimination between the pixels of the vessel and the background. For the heading, additional information has to be extracted to solve the direction ambiguity of the main orientation of the bounding box. A common approach for this is the vessel wake analysis, from which the sailing direction and information about the motion of the vessels can be obtained. This approach usually considers the azimuth offset of the vessel with respect to the vertex of its wake in order to estimate the heading and range velocity of the vessel [Peng et al., 1996; Tunaley, 2003; Radius and Marques, 2008]; in this way, it exploits the well-known phenomenon of azimuth shifts of a moving target in the SAR image due to its motion in range direction [Raney, 1971]. In addition, the analysis of the shape of the wake alone is another option to estimate the direction and velocity of the vessel [Zilman et al., 2004]. However, these techniques are limited to the presence of the vessel's wake, which is not always visible in the SAR images. Other more general approaches to estimate the velocity and heading of the vessels are based on the analysis of the received radar signal of moving targets; in particular, the analysis of the Doppler spectra of the vessels is often used in the estimation of their range-velocities. This technique has been reported to provide a good agreement with ground-truth data for spaceborne acquisitions [Dragosevic et al., 2008; Brusch et al., 2011; Renga and Moccia, 2014], so it can be used as a tool to extract information about the motion of the vessels.

An additional problem of SAR images of moving targets is the likely presence of aberrations such as defocus [Raney, 1971]. In the case of vessels, their motion may induce these artefacts that affect the quality of their image, and as a consequence, undermine the extraction of geometrical features such as their dimensions and main orientation. In order to overcome this problem, autofocus of the vessels' SAR signatures is required to compensate their defocus; examples of these procedures on spaceborne SAR acquisitions have been shown by Martorella et al. [2012] using an inverse SAR approach to refocus SLC spotlight images of vessels, or Santamaria et al. [2014] who use classical autofocus techniques on SLC vessels' signatures from stripmap acquisitions. By improving the focusing of the vessels' SAR signatures, better estimates of their features could be obtained.

In this paper, an automatic processing chain has been implemented to explore the potential of using spaceborne single-look complex (SLC) SAR images of vessels for automatic

feature extraction, namely their dimensions and heading, which is often information of interest in maritime surveillance systems. The SLC stripmap data have been selected because it allows the use of advanced post-processing techniques that require the phase information. Moreover, in comparison to acquisition modes such as spotlight or scanSAR, stripmap offers a good trade-off between image resolution and swath extension, which is a requirement in any monitoring application. The inputs of the algorithm presented are the SLC chips from detected vessels. They are obtained using the Wavelet-Transform Vessel Detection tool developed at the Universitat Politècnica de Catalunya (UPC) [Tello et al., 2005]. An autofocus module is implemented to enhance the quality of the vessels' SAR signatures in order to obtain better outlines of their contours and estimates of the dimensions and main orientation.. In addition, the likely sailing direction of the vessel, i.e. the heading, is obtained by the Doppler analysis of the received radar signal by assuming vessels to be slow-moving targets. The whole processing chain is intended to be automatic, so it can be used as an add-on module for the post-processing of a large number of detected vessels. The scope of this paper is to provide the outline of the whole processing chain and preliminary results using real RADARSAT-2 acquisitions.

This paper is organized as follows. The first section provides a brief overview of the feature extraction algorithm. The masking process used to isolate the vessels' SAR signatures from the background is described in the second section. The third section addresses the application of the autofocus technique in the SAR signatures. The fourth section is devoted to the extraction of the dimensions and heading of the vessels. The preliminary results are presented in the fifth section using SLC chips from RADARSAR-2 acquisitions. The conclusions are presented at the end of this paper.

Overview of the feature extraction algorithm

This feature extraction algorithm is intended to be applied to SAR images of the detected vessels. Chips of SLC images from spaceborne stripmap acquisitions are considered as the inputs. The basic block diagram of the processing chain is shown in Figure 1. The main steps of the process can be summarized as follows: 1) a SLC chip containing a single vessel is selected as the input. 2) A masking process is applied to select the range bins that contain the SAR signature. 3) The range and ground-range velocity is estimated from the Doppler analysis using techniques such as Energy Balancing (EB) [Bamler, 1991] or Correlation Doppler Estimator (CDE) [Madsen, 1989]. 4) The autofocus procedure (e.g., Phase Gradient Autofocus (PGA) [Eichel et al., 1989] or Multiple Aperture Mapdrift (MAM) [Carrara et al., 1995]) is applied in azimuth to the signature to improve its image quality. 5) The enhanced SAR signature of the vessel is isolated from the sea clutter and a bounding box is computed. Finally, 6) the dimensions of the vessel are computed from the Universal Transverse Mercator (UTM) projection of the bounding box, and the heading ambiguity is solved with the direction of the ground range-velocity.

Masking

The masking of the SAR signature is used to automatically identify the range bins and the area that belongs to the SAR signature of the vessel. It is a previous step of both the application of the autofocus and the feature extraction.

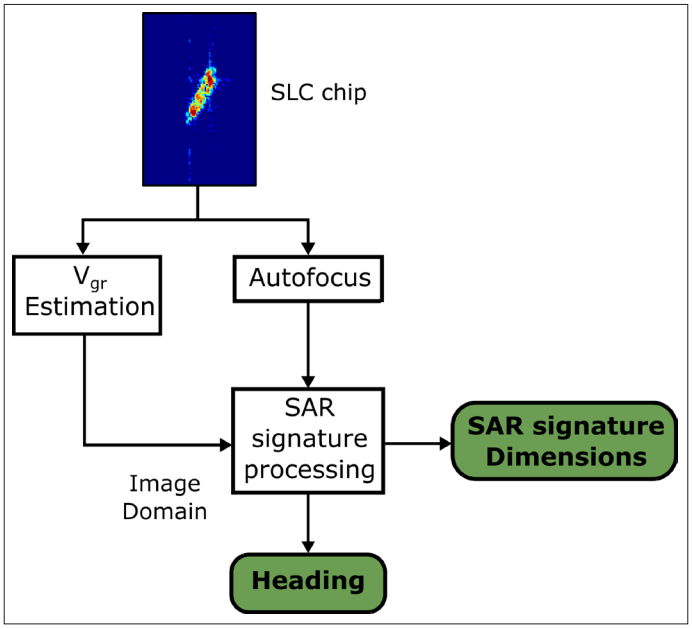

Figure 1 - Basic block diagram of the processing chain for the automatic feature extraction.

In the algorithm, the masking process is based on the automatic selection of an intensity threshold since the inputs come from single-channel images. The high reflectivity of the vessel signature is exploited to discriminate the pixels that likely belong to the target from those of the sea clutter. A statistical distribution is used to model the reflectivity of the sea clutter in the SLC chip. Distributions such as K, Weibull, and Log-normal are well-known for modelling the reflectivity (in amplitude) of the sea clutter in SAR images [Ward et al., 2006]. In this algorithm, the log-Weibull distribution has been used in order to work directly with the intensity images in dB. On the one hand, it has been observed that this model presented a better agreement with the distribution of the sea clutter intensity than the log-Normal distribution in the high-resolution SLC SAR images analysed. On the other hand, the log-Weibull model offers the advantage of simpler mathematical tractability (in comparison with the K distribution, for instance). This makes the practical computation of their parameters easier by fitting its cumulative distribution function to the empirical data using advanced optimisation routines (based on the gradients) in high-level programming languages like MatLab and IDL/ENVI.

The a priori knowledge of the content of the input image makes the computation of the mask easier. It is assumed that there is only one vessel per image and that most of the pixels belong to the sea clutter. Then, a rough estimate of the parameters of the log-Weibull model is done considering the whole image. With a relaxed probability of false alarm (PFA), e.g. PFA = 0.05, the brighter pixels are selected, and the main cluster is obtained after the application of morphological operations [Haralick et al., 1987]. In the presented masking process, the morphological operations of opening and closing are used as filter mechanisms for the "salt and pepper" noise removal in the binary images [Ritter et al.,

2000]. The opening and closing operations involves successively applying the two basic morphological operations of dilation and erosion using a structuring element (SE); this SE is the shape that interacts with the clusters and is directly related to the modification of their details after the application of an operator. Basically, the opening operation (eroding + dilating) aims to suppress image details smaller than the SE while preserving the shape of unfiltered features; on the other hand, the closing operation (dilating + eroding) aims to fill holes and narrow gaps smaller than the structuring element [Ritter et al., 2000]. In the presented processing, a structuring element of 2x2 pixels is used for the opening and closing. Thus, after the intensity thresholding, isolated single pixels and small clusters are discarded, whereas small holes and gaps are filled. As a result, a smoother and cleaner mask is obtained. This preliminary mask is used to roughly separate the pixels that belong only to the sea clutter, using them to estimate once more the parameters of the statistical model.. The final mask for the vessel's SAR signature is obtained with a more restrictive PFA, e.g. PFA=10^{-5}, with the refined model of the statistics of the sea clutter intensity and the application, again, of the morphological operations. This final process is depicted from left to right in Figure 2.

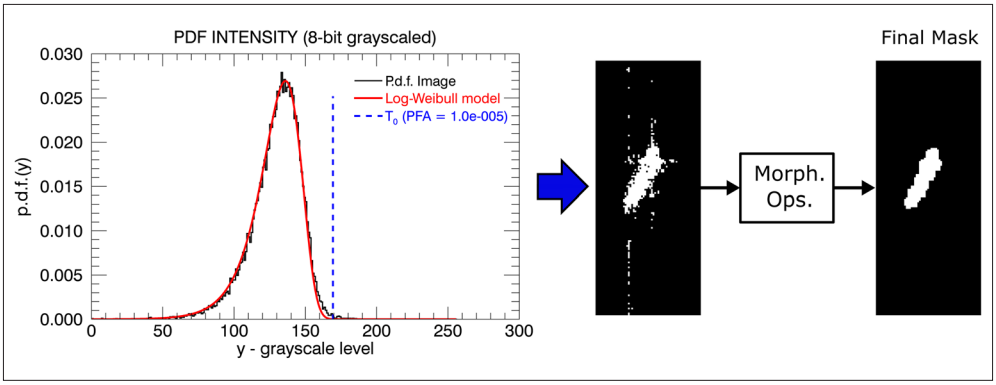

Figure 2 - Process of computation of the final mask for the SAR signature: (left) thresholding of the brighter pixels based on a given PFA and the statistical model of the sea clutter intensity; (centre) direct mask after the thresholding; (right) final mask after the application of morphological operations (opening and closing).

Autofocus step

The SAR processing is based on the application of matched filtering in both range and azimuth dimensions to obtain the final image. In the range dimension, this process is straight forward due to the complete knowledge of the generated radar pulse signal. In contrast, in the azimuth dimension, it relies on the modelling of the range variation during the extension of the synthetic aperture. Thus, discrepancies between this model and to the actual evolution of the range introduce phase errors, whose quadratic and higher order terms produce the most severe deterioration by defocusing the SAR image [Raney, 1971; Carrara et al., 1995].

In the case of stripmap images from spaceborne SAR sensors, some assumptions can be made in the analysis of the expected motion of the vessels and the phase errors in their

received radar signal. First, the platform trajectory in this type of acquisition is virtually stable, so it can be assumed that, after the processing of the image with the proper Doppler rate and Doppler centroid, localized blurring artefacts are mainly produced by targets in motion. Secondly, the typical sailing speed of medium/large vessels is a lot lower than the speed of the sensor's platform, so the vessels can be considered slow-moving targets. In these conditions, the scatterers of the vessels are assumed to remain mainly in the same range resolution cell during the effective observation time for stripmap acquisitions. Thus, its signature is expected to be deteriorated more significantly in the azimuth direction, in particular, by its range acceleration component which modifies the expected Doppler rate [Raney,1971]. This change in the Doppler rate translates into blurring effects that are commonly observed along the azimuth direction of the vessels' SAR signatures in maritime images. In this paper, local application of the autofocus techniques in azimuth direction is considered in order to enhance the quality of the SAR signatures of the vessels, which can be used later to extract a more reliable estimation of its features.

The aim of the autofocus techniques is to automatically improve the focus of the final image by estimating the phase errors from the SAR signal, and then, applying the respective error compensation. Second and higher order phase errors are usually the ones that the autofocus techniques look to compensate since they are responsible for the most severe deterioration of the SAR image [Carrara et al., 1995]. In this algorithm, three widely used autofocus techniques were implemented to compensate the defocus in the azimuth direction: phase gradient autofocus (PGA) [Eichel et al., 1989], multiple aperture mapdrift (MAM) [Carrara et al.,1995], and an image contrast based autofocus (ICBA) [Cumming et al., 2015]. PGA follows a non-parametric approach; it does not assume an explicit model of the phase error function, which means that it could compensate arbitrary high order phase errors. PGA estimates the gradient of the phase error as a function of the aperture time of the received SAR signal, so the phase error is obtained through the integration of this gradient with respect to the time. In contrast, MAM follows the model-based approach by assuming an a priori polynomial function to model the phase error; then, it analyses iteratively the relative shifts between (two or more) non-overlaping subapertures from which the coefficients of the polynomial phase error function can be derived. The ICBA technique implemented also uses the model-based approach, and the idea is to apply a multidimensional optimisation to get the polynomial coefficients of the phase error function that maximizes an objective function related to the contrast of the image.

The common implementation of the autofocus techniques assumes that the same phase error affects the whole image. But in some cases, large vessels may present different defocus along the range bins due to their rotational motion. Thus, the processing algorithm allows the user to select the application of the autofocus techniques as a single function obtained from all the range bins or in an independent range-bin (IRM) mode; the latter is proposed in this implementation to overcome the variation of the defocus in the SAR signature along the range direction. In the IRM mode, each range bin is considered independently, so a phase error function is obtained and compensated for each range bin of the vessel's SAR signature. Figure 3 shows an example of a typical SAR signature of a vessel with defocus artefacts and the refocused image by using the MAM technique in the IRM mode; the peak value intensity is increased by 3.61 dB, and the different defocus along the range direction is compensated.

Feature extraction: dimensions and heading

Dimensions

The automatic extraction of the dimensions of the vessels is done directly on the intensity image. First, it requires the isolation of the SAR signatures from the sea clutter; then, the computation of the corresponding bounding box from which the dimensions are computed. This basic geometry is assumed because most of the SAR signatures of medium/large vessels observed in SAR images tend to appear as quasi-rectangular shapes.

Once the autofocus has been done, the enhanced SAR signature is extracted by masking the sea clutter. The signature is used to compute the main orientation of the distribution of the pixels by using the Principal Component Analysis (PCA) approach [Jollifre, 2002]; with the computation of the centre of mass, the main and secondary axes of the box are obtained. These axes are used as the references to compute the sides of the box that fits the contour of the signature of the vessel. Finally, the locations of the vertices of the bounding box are mapped to UTM coordinates, and the dimensions in the ground projection are computed (Fig. 4).

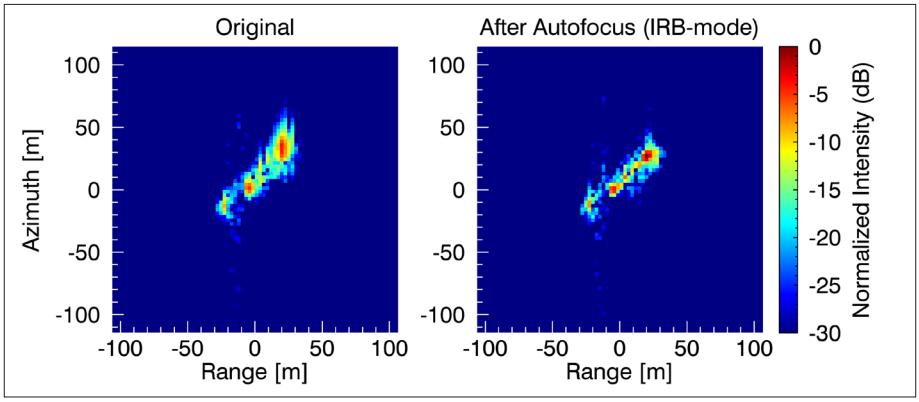

Figure 3 - Example of the refocus of a vessel's signature applying the MAM technique (in IRB mode). (Left) Original SLC chip; (right) SLC chip after autofocus. Dynamic range of 30 dB. Intensity normalized with respect to the maximum value of the refocused image.

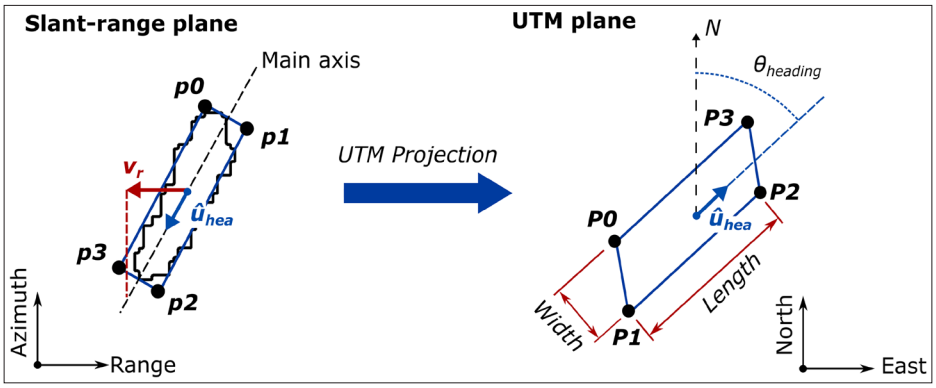

Figure 4 - Diagram of the computation of the dimensions and heading of the vessel from its bounding box and the direction of its ground-range velocity.

Heading

The main axis of the bounding box provides the orientation of the vessel at the moment of the SAR acquisition. Nevertheless, the heading still needs to be defined in an unambiguous way. Instead of analysing the reflectivity of the SAR signature or the wake to determine the bow and stern of the vessel, the motion of the vessel is exploited, in particular, its ground-range velocity.

In typical conditions of a travelling vessel, it can be assumed that its translational motion is more significant in the horizontal plane than in the vertical direction. Consequently, the ground-range velocity component of the vessel could be seen as the most significant contributor to the induced range velocity. It is a well-known effect that a range velocity component appears as a linear term in the phase history of the SAR signal [Raney, 1971], causing a shift in the Doppler centroid frequency of:

$$\Delta f_{DC} = \frac{2v_r}{\lambda} \quad [1]$$

with v_r as the range velocity component, and λ the wavelength of the carrier frequency of the SAR sensor. Thus, a measure of this component is obtained from the Doppler analysis of the SAR signal of the vessel by using methods of fractional Doppler centroid estimation such as Energy Balancing (EB) [Bamler, 1991] or Correlation Doppler Estimator (CDE) [Madsen, 1989]. With the assumption that the vessel is moving mainly in its horizontal plane, the direction of is used to determine the direction of the unitary vector $\hat{u}_{hea}$, which is associated to the main axis of the bounding box as shown in Figure 4. Then, its UTM projection allows obtaining the heading of the vessels with respect to the North. There is the intrinsic assumption that the ground-range velocity of the vessel, v_g , is proportional to v_r. In this paper, only the direction of v_r is used as indicator of the likely of motion of the vessel due to two factors: 1) in real conditions, the motion of the vessels could be more complex than the one assumed, which could affect the magnitude of the ground-range velocity, although it can be expected that at least its direction remains correct; and, 2) the relation of Δf_{DC} and v_r in Equation [1] is expected to be only an approximation when using SLC images due to the suppression of part of the Doppler spectra in the windowing process of the image formation [Cumming et al., 2015]. Thus, the magnitudes of v_r and the estimated Δf_{DC} would not be truly proportional in this case.

Preliminary results

The feature extraction algorithm was tested with experimental SLC data. For this, the inputs are SLC chips from stripmap SAR data acquired during the campaigns of the European Project NEREIDS [Margarit, 2013]. They belong to RADARSAT-2 HH-stripmap acquisitions done in 2014 near the coast of Ålesund, Norway, with Range-Azimuth resolution of around 2.6m x 2.7m (or, Ground-range-Azimuth resolution of around 3.7m x 2.7m); Table 1 summarizes the main acquisition parameters of these images. Five SLC chips of SAR signatures of vessels were selected due to the available ground-truth data. Their positions in the geocoded image were positively cross-checked with the AIS information at the time of the SAR acquisition.

Table 1 - Main parameters of RADARSAT-2 acquisitions.

Parameter	Value
Mode	SLC stripmap
Channel	HH
Location	Ålestund, Norway
Carrier frequency	5.40 GHz
Azimuth resolution	2.46 m - 2.99 m
Range resolution	2.66 m
Ground-range resolution	3.57 m - 3.92 m
Incidence angle	42.7° - 48.2°

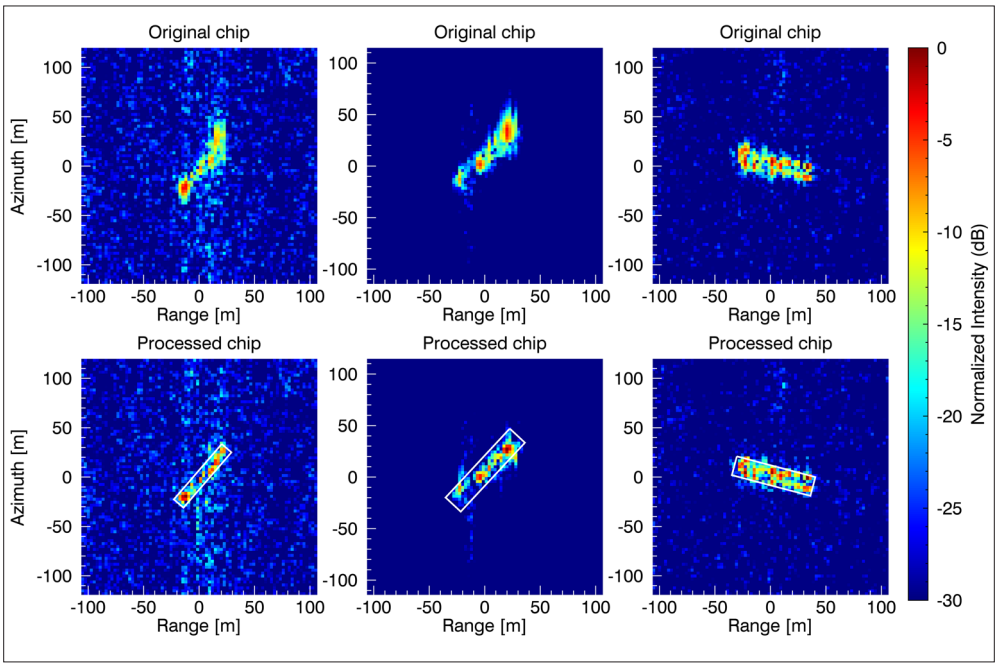

Figure 5 - Input SLC chips number 1, 2, and 3 (top row), and their respective output after the application of the processing chain (bottom row). Dynamic range of 30 dB. Intensity normalized with respect to the maximum value of the processed images for each pair of SLC chips.

Figure 5 shows three of the input SLC chips employed along with their respective outputs after the application of the algorithm. The autofocus processing (MAM) has improved the vessels' SAR signatures by better concentrating the energy of the scatterers in the azimuth direction, obtaining a signature that resembles more the typical quasi-rectangular shapes. In addition, a visual inspection of the bounding boxes shows that their dimensions and main orientations correspond to the distribution of the improved SAR signatures, which is crucial in order to get a good estimation of these parameters. Table 2 contains the results of the extracted data after processing the five chips and their respective AIS information at the

time of the respective acquisitions. The estimates of the ground-range velocity, using the EB and CBE techniques are also included in this Table, but only to show the agreement with the actual value obtained from the AIS information. The absolute errors of these estimated features are presented in Table 3.

Table 2 - AIS data and the feature extracted after processing the SLC chips.

AIS Data					
Chip number	**Heading [°]**	**Length [m]**	**Width [m]**	**v_g [m/s]**	**IMO number**
1	50	89	12	-3.31	9145140
2	44	93	15	5.38	9334404
3	97	94	17	-2.78	9432646
4	241	78	17	-4.95	9617973
5	212	119	19	-3.46	9272735
Extracted data from processing					
Chip number	**Heading [°]**	**Length [m]**	**Width [m]**	**EB v_g [m/s]**	**CDE v_g [m/s]**
1	55.4	84.6	14.8	-5.77	-4.54
2	39.9	103.0	22.5	8.87	8.85
3	110.0	103.6	20.1	-4.21	-3.57
4	234.2	89.7	26.4	-3.59	-4.28
5	208.4	127.3	43.7	-0.8	-2.61

Table 3 - Absolute error, $|Data_{extracted} - Data_{AIS}|$, between the extracted features and the AIS data.

Absolute error					
Chip number	**Heading [°]**	**Length [m]**	**Width [m]**	**EB v_g [m/s]**	**CDE v_g [m/s]**
1	5.4	4.4	2.8	2.46	1.23
2	4.1	10.0	7.5	3.49	3.47
3	13.0	9.6	3.1	1.43	0.79
4	6.8	11.7	9.4	1.36	0.67
5	3.6	8.3	24.7	2.66	0.85
μ_e	6.9	8.8	9.5	2.3	1.4
σ_e	3.4	2.5	8.0	0.80	1.1

In general, the dimensions and heading extracted were similar to the ground-truth information for this small dataset. Having the input images Ground-range-Azimuth resolution of around 3.7m x 2.7m, an average error of 8.8m and 9.5m were obtained for the length and width of the vessels, respectively; for the heading, the average error was 6.9°; for the ground-range velocities, the average errors were 2.3m/s and 1.4m/s using the EB and CDE techniques,

respectively. These results suggest that 1) the dimensions of the vessels could be inferred (approximately) from the dimensions of their processed SAR signatures despite the defocus aberrations of the original images; the dimensions of the vessels have been overestimated in most of the cases, and this could be attributed to artefacts that may broaden the extracted contour of the SAR signatures like the vessel-sea reflections and secondary lobes from highly reflective scatterers. 2) The statistical model used for the sea clutter was a good descriptor of its intensity distribution in the processed SLC chips, allowing the computation of a mask that fits closely the contours of the vessels' SAR signatures. And, 3) solving the orientation ambiguity with the direction of the ground-range velocity of the vessels is a simple and effective approach for determining their heading, and no further analysis of their reflectivity distribution or their wakes (which are not always visible) is required for identification of the stern and bow of the vessels.

Due to the loose assumption of the simplified motion of the vessel and the use of SLC data, it was expected that the magnitude of the ground-range velocities would show only a similar trend to the ground-truth data. The motion of a vessel is far more complex in reality, presenting translational and rotational motions over their three axes; this means that its range velocity component is, in fact, the result of the combination of all these motions. As a consequence, the estimated range velocity can only be considered an approximation of the real motion of the vessel. On top of that, using SLC data implies that the vessel's azimuth spectrum has already been modified and partially suppressed of during the image formation. By comparing both estimation techniques for the Doppler centroid frequency, similar results were obtained for the ground-range velocity, although the estimates from the CDE tended to be closer to the ground-truth data. This can be attributed to the sensitivity of the EB technique to asymmetries in the Doppler spectrum envelopes of the vessels' Doppler spectra and their modifications due in the SLC image formation.

Conclusions

Spaceborne SAR technology is an attractive candidate as an external source of information for vessel surveillance systems. It provides high resolution imaging at a global scale regardless of the weather conditions and natural illumination. In this paper, a processing chain has been implemented to explore the potential of using single-look complex (SLC) SAR images from stripmap acquisitions to extract information of interest about the vessels. The convenience of using SLCs is due to its availability and post-processing capabilities; all civilian spaceborne SARs can provide it, and as a consequence, the revision time of an area is not tied to a specific type of SAR sensor. Moreover, the stripmap mode offers a practical advantage regarding the acquisition of high-resolution images of areas of tens of kilometres, which makes its suitable for expanding the coverage of the surveillance systems.

The SLC chips containing the SAR signatures of the vessels were processed to automatically obtain their dimensions and heading. The defocusing distortions due to motion of the vessel were compensated by the local application of autofocus techniques such as PGA or MAM, improving the quality of the SAR signatures. The combination of the automatic selection of an intensity threshold and morphological operations provided a quick way to effectively isolate the SAR signatures of the vessels based on their reflectivity. Then, from their bounding boxes, their dimensions are extracted. The heading ambiguity was solved

by the analysis of the effects of the motion of the vessels on their respective SAR signals. The processing chain was tested with five SLC chips from a RADARSAT-2 stripmap image. The preliminary results are closely related to the values of the ground-truth data given by the AIS information near the time of the respective acquisitions. The dataset used is small and analysis with more examples is required for a complete characterization of the algorithm. Nevertheless, the results are encouraging for the use of the presented processing chain as a tool for the automatic extraction of information of any number of detected vessels in stripmap SLC SAR images.

Acknowledgements

This research work has been financed by the Spanish Science, Research and Innovation Plan (Ministerio de Economía y Competitividad) with Project Code TIN2014-55413-C2-1-P, the European Commission under project NEREIDS (FP7-SPACE-2010-1 contract 263468), and the Generalitat de Catalunya (AGAUR grant FI-DGR-2012-LY080095).

References

Bamler R. (1991) - *Doppler frequency estimation and the Cramer-Rao bound*. IEEE Transactions on Geoscience and Remote Sensing, 29 (3): 385-390. doi: http://dx.doi.org/10.1109/36.79429.

Brusch S., Lehner S., Fritz T., Soccorsi M., Soloviev A., Van Schie A. (2011) - *Ship Surveillance With TerraSAR-X*. IEEE Transactions on Geoscience and Remote Sensing, 49 (3): 1092-1103. doi: http://dx.doi.org/10.1109/TGRS.2010.2071879.

Carrara W.G., Majewski R.M., Goodman R.S. (1995) - *Spotlight Synthetic Aperture Radar: Signal Processing.* Artech House Remote Sensing Library.

Crisp D.J. (2004) - *The state-of-the-art in ship detection in synthetic aperture radar imagery*. Technical Report DSTO-RR-0272, Chief, Intelligence, Surveillance and Reconnaissance Division.

Cumming I.G., Wong F.H. (2005) - *Digital Processing of Synthetic Aperture Radar Data: Algorithms and Implementation.* Artech House Remote Sensing Library.

Dragosevic M.V., Vachon P.W. (2008) - *Estimation of Ship Radial Speed by Adaptive Processing of RADARSAT-1 Fine Mode Data.* IEEE Geoscience and Remote Sensing Letters, 5 (4): 678-682. doi: http://dx.doi.org/10.1109/LGRS.2008.2002433.

Eichel P.H., Ghiglia D.C., Jakowatz C.V. (1989) - *Speckle processing method for synthetic-aperture-radar phase correction*. Optics Letters, 14 (1): 1-3. doi: http://dx.doi.org/10.1364/OL.14.000001.

Estable S., Teufel F., Petersen L., Knabe S., Saur G., Ullmann T. (2009) - *Detection and classification of offshore artificial objects in TerraSAR-X images: First outcomes of the DeMarine-DEKO project*. OCEANS 2009 - EUROPE, Bremen, pp. 1-8. doi: http://dx.doi.org/10.1109/OCEANSE.2009.5278298.

European Commission (2015) - *Vessel monitoring system (VMS)*. Available online at: http://ec.europa.eu/fisheries/cfp/control/technologies/vms/index_en.htm.

International Maritime Organization, IMO (2015) - *Automatic Identification Systems (AIS)* Available online at:: http://www.imo.org/en/OurWork/Safety/Navigation/Pages/AIS.aspx.

Haralick R.M., Sternberg S.R., Zhuang X. (1987) - *Image Analysis Using Mathematical*

Morphology. IEEE Transactions on Pattern Analysis and Machine Intelligence, PAMI-9 (4): 532-550. doi: http://dx.doi.org/10.1109/TPAMI.1987.4767941.

Jollifre I.T. (2002) - *Principal Component Analysis*. Springer Series in Statistics.

Madsen S.N. (1989) - *Estimating the Doppler centroid of SAR data.* IEEE Transactions on Aerospace and Electronic Systems, 25 (2): 134-140. doi: http://dx.doi.org/10.1109/7.18675.

Margarit G. (2013) - *Integrated maritime picture for surveillance and monitoring applications*. IEEE International Geoscience and Remote Sensing Symposium (IGARSS): 1517-1520, 21-26 July 2013. doi: http://dx.doi.org/10.1109/IGARSS.2013.6723075.

Martorella M., Giusti E., Berizzi F., Bacci A., Mese E.D. (2012) - *ISAR based techniques for refocusing non-cooperative targets in SAR images*. IET Radar, Sonar & Navigation, 6 (5): 332-340. doi: http://dx.doi.org/10.1049/iet-rsn.2011.0310.

Peng C.Y., Liu A.K., Chang S.Y.S. (1996) - *Detection and analysis of ship waves in ERS-1 SAR imagery*. Geoscience and Remote Sensing Symposium, IGARSS '96 'Remote Sensing for a Sustainable Future', International, Lincoln, NE, 1: 380-382. doi: http://dx.doi.org/10.1109/IGARSS.1996.516347.

Radius A., Marques P. (2008) - *A Novel Methodology for Full Velocity Vector Estimation of Ships Using SAR Data.* Proceedings of 7th European Conference on Synthetic Aperture Radar (EUSAR), Friedrichshafen, Germany, pp. 1-4.

Tello M., Lopez-Martinez C., Mallorqui J.J. (2005) - *A novel algorithm for ship detection in SAR imagery based on the wavelet transform.* IEEE Geoscience and Remote Sensing Letters, 2 (2): 201-205. doi: http://dx.doi.org/10.1109/LGRS.2005.845033.

Raney R.K. (1971) - *Synthetic Aperture Imaging Radar and Moving Targets.* IEEE Transactions on Aerospace and Electronic Systems, AES-7 (3): 499-505. doi: http://dx.doi.org/10.1109/TAES.1971.310292.

Renga A., Moccia A. (2014) - *Ship velocity estimation by Doppler Centroid analysis of focused SAR data*. IEEE Geoscience and Remote Sensing Symposium, Quebec City, QC, pp. 1809-1812. doi: http://dx.doi.org/10.1109/IGARSS.2014.6946805.

Ritter G.X. Wilson J.N. (2000) - *Handbook of Computer Vision Algorithms in Image Algebra*. CRC Press, 2nd (Ed.).

Santamaria C., Cicuendez Perez J., Greidanus H., Broussolle J. (2014) - *Improvement of maritime target signatures in satellite SAR images.* Proceedings of 10th European Conference on Synthetic Aperture Radar (EUSAR), Berlin, Germany, pp. 1-4.

Saglianò D., Musetti L., Cataldo D., Baruzzi A., Martorella M. (2014) - *Fast detection of maritime targets in high resolution SAR images.* IEEE Radar Conference, Cincinnati, OH, pp. 0522-0527. doi: http://dx.doi.org/10.1109/RADAR.2014.6875647.

Tunaley J.K.E. (2003) - *The estimation of ship velocity from SAR imagery*. IEEE International Geoscience and Remote Sensing Symposium, IGARSS '03, 1: 191-193 doi: http://dx.doi.org/10.1109/IGARSS.2003.1293720.

Ward K.D., Watts S., Tough R.J.A. (2006) - *Sea clutter: scattering, the K-distribution and radar performance*. Volume, 20 IET, 2006.

Zhang H., Tian X., Wang C., Wu F., Zhang B. (2013) - *Merchant Vessel Classification Based on Scattering Component Analysis for COSMO-SkyMed SAR Images.* IEEE Geoscience and Remote Sensing Letters, 10 (6): 1275-1279. doi: http://dx.doi.org/10.1109/LGRS.2012.2237377.

Zilman G., Zapolski A., Marom M. (2004) - *The speed and beam of a ship from its wake's SAR images*. IEEE Transactions on Geoscience and Remote Sensing, 42 (10): 2335-2343. doi: http://dx.doi.org/10.1109/TGRS.2004.833390.